Article

Chinese Science Bulletin

Engineering Thermophysics

September 2011 Vol.56 No.26: 2862–2868
doi: 10.1007/s11434-011-4630-9

Premixed jet flame characteristics of syngas using OH planar laser induced fluorescence

YANG Li[1], WANG ZhiHua[1*], ZHU YanQun[1], LI ZhongShan[2], ZHOU JunHu[1], HUANG ZhenYu[1] & CEN KeFa[1]

[1] *State Key Laboratory of Clean Energy Utilization, Zhejiang University, Hangzhou 310027, China;*
[2] *Division of Combustion Physics, Lund University, Lund, P.O. Box 118, S-22100, Sweden*

Received October 14, 2010; accepted June 8, 2011

Lean premixed flame characteristics of several typical low calorific value (LCV) syngases (basis $CO/H_2/CH_4/CO_2/N_2$), including bituminous coal, wood residue, corn core, and wheat straw gasification syngas, were investigated using OH planar laser induced fluorescence (PLIF) technology. OH radical distributions within the turbulent flame were measured for different turbulence intensities. Flame structures of syngases were analyzed and characterized with respect to burnt and unburnt regions, flame curvature (sharp cusp), local extinction (holes and penetration), OH reaction layer thickness, wrinkling, and other features, with OH-PLIF instantaneous images and statistical analysis. Results show that H_2 content, LCV, and turbulence intensity are the most effective factors influencing the OH radical intensity and thickness of OH radical layers. The bituminous coal gasification syngas with relatively higher LCV and H_2 content tends to burn out easily. Through changes in thickness of the OH radical layers and signal intensities, the reaction layer can be compressed by intensifying turbulence and thereby the combustion processes of syngas.

PLIF, LCV, syngas, OH, jet flame

Citation: Yang L, Wang Z H, Zhu Y Q, et al. Premixed jet flame characteristics of syngas using OH planar laser induced fluorescence. Chinese Sci Bull, 2011, 56: 2862–2868, doi: 10.1007/s11434-011-4630-9

The integrated gasification combined cycle is one of the more-promising clean and efficient electricity generation technologies at present for coal utilization. Coal is partially oxidized to provide the needed heat for the endothermic gasification at a relatively high temperature and pressure, and the residue is translated into syngas fuel in the gasifier. The syngas, consisting mainly of CO, H_2, CH_4, is burned in a gas turbine to generate electricity after purification. The downstream waste-heat-recovery steam-turbine system further improves the overall energy conversion efficiency, which is much higher than a direct coal-combustion steam-turbine system [1]. As a kind of renewable and carbon-neutral fuel, biomass has attracted much more attention world-wide recently. Combustion, gasification, and liquefaction are the most popular utilization methods for biomass [2].

Syngas, derived from coal and biomass gasification, is considered to be a more attractive fuel for further energy conversion and utilization. However, the LCV of syngas is usually much lower than for natural gas because of the dilution of N_2 and CO_2. Efficient utilization of LCV syngas not only can enhance energy utilization efficiency but also can reduce toxic emissions, such as CO_2, compared with just coal combustion. Coal and biomass can be used more cleanly and efficiently through gasification, which is of great significance both for environment, economic and energy security [3]. The combustion and flame stability of syngas, though, will be a big problem because of the variation of gas composition derived from the operation parameters of gasifier. The characteristics of syngas are always determined by different kinds of gasification fuels, such as the type of coal and biomass, gasification oxidizer such as steam, air, and pure oxygen. Therefore, it is necessary to investigate the

*Corresponding author (email: wangzh@zju.edu.cn)

combustion property and the flame characteristic of LCV syngas in depth.

Several prior studies on LCV syngas combustion have been reported [4–7] that were mainly focused on flame stability, flame extinction limits, laminar flame speed, NO_x and CO emissions, dilution swirling diffusion flame, and other aspects. Choudhuri and Subramanya [8] studied the flame extinction limits of H_2-CO fuel blends. Goch and Chadwick [9] measured NO emission of CO-H_2-CH_4 premixed flame. Dobbeling and Eroglu [10] analyzed the feasibility of low NO_x premixed combustion of MBtu fuels under industrial gas turbine conditions. Ouimette and Seers [11] investigated laminar flame speeds within methane and wood residue syngas using a CCD camera. Natarajan and Lieuwen [12] studied the effect of CO_2 dilution, preheat temperature and pressure on the laminar flame speeds of H_2/CO mixtures.

However, most of the above-mentioned studies had focused on diffusion flames at stoichiometric and fuel rich conditions, whereas in practical low emission combustion facilities, such as gas turbines, lean premixed flames were the major combustion mode. Several studies have claimed combustion of syngas but the gas compositions were just binary mixtures of H_2 and CO, whereas actual gas compositions of syngas are more complex with the inclusion of CO_2, CH_4, O_2, complex hydrocarbons, N_2, and other species. Therefore, several lean premixed jet flames fueled by typical LCV syngas including the just-mentioned species were investigated in this paper using advanced planar laser induced fluorescence (PLIF) diagnostic technology. The structures within the well-developed jet flame and turbulence-flame interactions were studied here. At the same time, typical methane/air flame was also employed for comparison and validation.

1 Experimental setup

Syngas fuels are typically composed of primary active components H_2 and CO, small amounts of CH_4 and higher-order hydrocarbons, and various amounts of non-combustible components like O_2, H_2O, N_2, and CO_2. The gas composition usually varies with operation parameters of the gasifier and the different kinds of fuels such as the various types of coal and biomass [13]. The LCV of syngas is usually 4000–13000 kJ/m^3, much lower than natural gas and methane, which is about 36000 kJ/m^3. Here, four LCV syngas types were selected based on gasification of bituminous coal, wood residue, corn core and wheat straw; the gas composition and LCV of each are summarized in Table 1.

Samples of the four LCV syngases were premixed with air and burned on a specific McKenna burner that is water-cooled and has a centered jet tube. A surrounding co-flow of CH_4-air lean premix (60 mm diameter) was used to isolate the central object flame from ambient air. The flow rates of methane and air were 3.0 L/min and 33.7 L/min, respectively, which were held constant by a mass flow controller. The central jet flow ($d = 2.3$ mm inner diameter) was a mixture of syngas and air with an equivalence ratio that varied from 0.6 to 1.0 and Reynolds number that varied from 5000 to 15000, corresponding to a velocity that varied from 35 to 105 m/s. The OH radical produced in the combustion process was imaged with PLIF technology.

The OH-PLIF measurement system consisted of a laser source, which included a Nd:YAG as pumping laser and a tunable dye laser, fluorescence detection using an intensified charge coupled device (ICCD) camera, and equipment for signal control and data acquisition. The flow diagram of the experimental setup was shown in Figure 1. The laser pulse for LIF excitation was generated by a second harmonic Nd:YAG laser (0.69 J@532 nm, YAG981E, Quantel), and a pumped dye laser (TDL90, Quantel) with a frequency doubler modified to 282.769 nm to excite the $Q_1(8)$ line of the $A^2\Sigma \leftarrow X^2\Pi(1,0)$ transition with pulse energy of about 0.007 J. A vertical laser sheet with a length of 37 mm was made by optical elements perpendicularly across the center of the jet flame. A 37 mm × 37 mm region was focused onto the ICCD camera (PI MAX II, Princeton Instruments) with a 512 × 512 pixel array through a UV lens (Nikon f/4.5). A narrowband filter (310FS10-50), which can get across the light with wavelength range of 305–315 nm, was used to obtain the OH fluorescence signal (about 308 nm) and eliminated the interference brought by the laser scattering and the flame background radiation. The ICCD camera, located perpendicularly with the laser sheet, operates with 50 ns gate width, 85 ns delay, and 10 Hz image sampling frequency synchronized with laser. To cover the downstream OH image of the flame, two position images were taken beginning 2 mm above the burner. Figure 2(a) illustrates the object positions of laser sheet and flame configuration with common digital camera (Nikon D80). Figure

Table 1 Gas composition of typical syngas with air blown gasification [8,14] a)

Type of syngas	Gas composition (%)						LCV (kJ/m^3)
	H_2	CO	CH_4	CO_2	N_2	O_2	
Bituminous coal	24.80	17.20	4.10	11.00	42.70	0	6300
Wood residue	13.98	20.20	3.95	9.15	52.02	1.20	5500
Corn core	12.30	22.50	2.32	12.50	48.98	1.40	5000
Wheat straw	8.50	17.60	1.36	14.00	56.84	1.70	3700

a)The LCV of H_2, CO and CH_4 are 10789, 12626, and 35796 kJ/m^3, respectively.

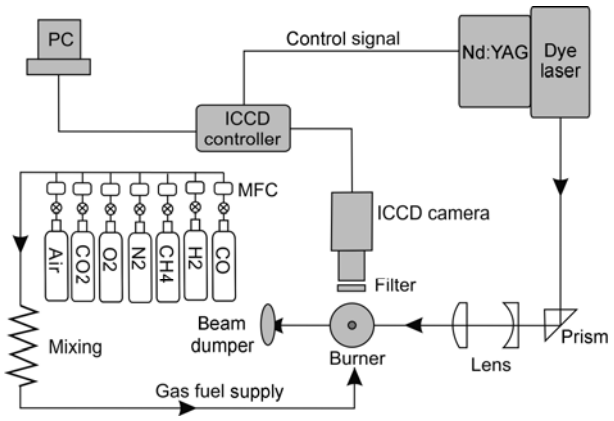

Figure 1 Schematic of the OH-PLIF measurement system (MFC: mass flow controller).

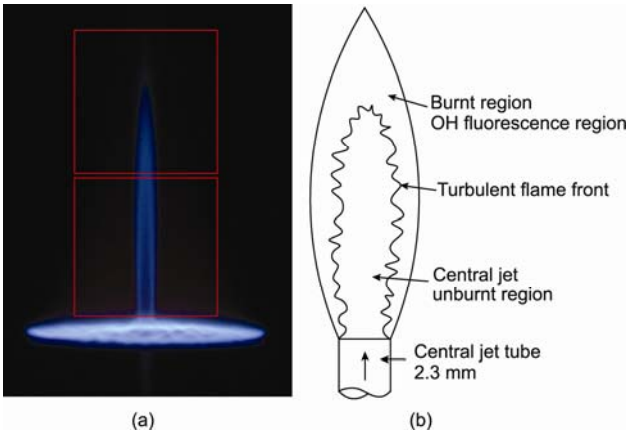

Figure 2 Turbulent flame. (a) Flame configuration and the two laser sheet locations and ICCD focus areas (red frames) imaged with a commercial digital camera; (b) a schematic diagram of turbulent flame structures.

2(b) illustrates the schematic diagram of turbulent flame structures, and various components of the flame such as flame front, central jet, burnt and unburnt region, OH fluorescence region have been indicated in the diagram. Post-processing including background subtracting and laser sheet intensity correction were conducted using MATLAB.

2 Results and discussion

OH is one of the most important intermediate radicals during combustion. As a good indicator of the flame region [15], OH has been widely used in laser diagnostic for flame front, structure and reaction zone visualization [16]. Here, two-dimensional OH radical distributions were imaged with PLIF technology for the four syngas samples (see Table 1).

2.1 Instantaneous OH images of the syngas jet flames

Figure 3 shows the instantaneous OH-PLIF images of jet flames of typical syngas samples along the axial distance 1*d*

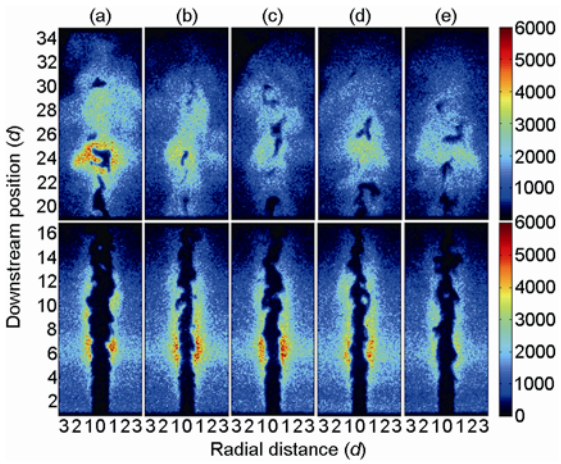

Figure 3 OH-PLIF instantaneous images of the syngas flames with Φ= 0.8 and Re = 10000. (a) Methane; (b) bituminous coal; (c) wood residue; (d) corn core; (e) wheat straw.

to 35*d* (*d* is the jet diameter, 2.3 mm) at equivalence ratio Φ= 0.8. In addition to the four syngas samples, a premixed methane/air sample was also conducted for comparison at the same condition. The order of images correspond to samples of from left to right methane/air, bituminous coal, wood residue, corn core and wheat straw. Based on jet velocity, diameter and viscosity of the gas mixture, Reynolds number of the flow condition was kept around Re = 10000.

As shown in Figure 3, spatially-folded structures associated with turbulence fluctuations were observed in the OH-PLIF images. The OH radical distribution was overall axially-symmetric about the axis of the central jet and decreased in the outer region, forming a taper. The region with the maximal intensity variation between the central jet and OH fluorescence regions was the flame front. For the stoichiometric and lean premixed flames, the hot or OH-containing regions were assigned to the burnt region and the others assigned to the unburnt region [17], and the combustion region of gas flame was considered not be effected by flame propagation due to the short reaction time scale [18]. Thus the OH radical distribution reflects the conjunction between burnt and unburnt regions.

In the lower part of the flame (downstream positions < 4*d* in Figure 3), the central jet flame layer was relatively smooth and of laminar style. While in the upper part of the flame (> 8*d*), the structure of the flame front was very irregular because of flame-turbulence. Turbulent eddies formed in the shear layers within the central jet can be observed from the instantaneous images. At downstream positions 20*d*–32*d*, large scaled turbulent structures and discontinuities in the OH distribution can be observed with ambient air infiltrated into the center of flame region. Many sharp cusps, folds and separate islands can be observed in the flame front, especially at downstream positions 6*d*–16*d*. Furthermore, some small holes can also be found in Figure 3(a), (d), and (e), corresponding to local quenching and re-ignition caused by

the flame curvature, as reported by Kalmthout et al. [19]. More detail information can be obtained with simultaneous measurements of OH, CH, HCO, formaldehyde, and other gas components.

Under similar conditions of equivalence ratio and turbulence intensity, some distinctive patterns can be observed between different fuels. In the lower parts of the flames, the OH radical intensity distribution for bituminous coal derived syngas was obviously stronger than that for wheat straw syngas, but similar to those for wood residue and corn core syngas. Furthermore, the central unburnt region of the wheat straw syngas flame was much wider than those of the others. The probable reason could be the lower LCV and the higher N_2 dilution in wheat straw derived syngas. Bearing in mind the limitation of the instantaneous information, quantitative processing of the images and detailed analysis will be discussed next.

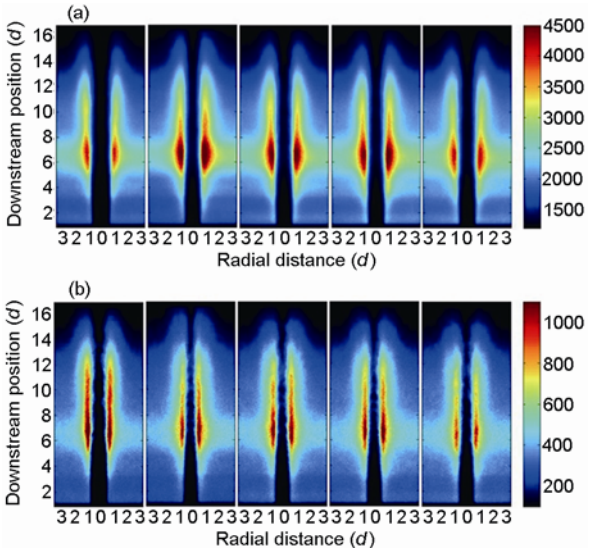

Figure 4 Statistically-evaluated OH-PLIF images of the syngas flames (a) ensemble average; (b) standard deviation. From left to right: methane, bituminous coal, wood residue, corn core, wheat straw.

2.2 Statistical analysis of turbulent premixed flame

The OH-PLIF instantaneous images can provide useful information about the combustion characteristics of syngas, such as flame location, flame structure, burnt and unburnt region, and local extinction. However, this provides only a qualitative description that is unable with just random instantaneous images to capture the intricacies of a turbulent jet flame subjected to turbulence fluctuations. Therefore, to further analyze the turbulent premixed flame, it is necessary to perform statistical analysis. Here, two statistics methods, namely ensemble averaging and standard deviation, were performed on 200 OH-PLIF single shot images for each sample.

With the same ordering as in Figure 3, Figure 4 shows the statistically-analyzed OH-PLIF images of typical LCV syngases and methane/air mixture. At the lower parts of the flames, (downstream positions <5*d* in Figure 4), relatively weak OH radical intensities were observed because of early-stage combustion and an uneven laser energy distribution. At downstream positions between 6*d*–8*d*, the OH signal intensity attained maximal values as well as maximum thickness in the reaction layers for all syngas and methane samples. As observed in comparing the panels in Figure 4(a), the unburnt regions in the central jet syngas flame were all narrower and the peak OH intensities were all higher than methane. Furthermore, the syngas had stronger OH radical intensities distribution regions compared to methane; the OH intensity can be judged easily by the color used here to indicate signal intensity. The probable reason for these phenomena was that syngas has a much lower LCV than methane that then affects combustion and flame structure.

There were no obvious pattern to be observed between the four syngas flames because these four types have similar LCV (<6500 kJ/m^3) and compositions. However, some minor differences still can be observed. In Figure 4(a), bituminous coal syngas is seen to have a relatively-stronger OH intensity distribution compared with others; wheat straw syngas had the lowest signal intensity level under similar conditions, while the signal intensities of wood residue and corn core syngas were intermediate. Two possible reasons are posited, and summarized as follows: first, the divergence of the heating values brings differences in heat release rates and consequently combustion temperatures; second, the H_2 molecules change greatly the diffusion of the flame front. Bituminous coal syngas has a much higher LCV (6300 kJ/m^3) than wheat straw syngas (3700 kJ/m^3); the LCVs for wood residue and corn core syngas were 5500 kJ/m^3 and 5000 kJ/m^3, respectively. Therefore, combustion temperatures and chemical reaction rates will be enhanced with the greater the heat release rate syngas fuel. Besides LCV, H_2 content in the fuel will be another major reason influencing combustion. Although methane has a much higher LCV (35800 kJ/m^3) than syngas (<6500 kJ/m^3), the averaged OH signal intensity was lower than for most syngases. The appearance of H_2 will greatly accelerate the burning velocity and combustion intensity. Our earlier work focusing on the effect of H_2 content on the flame structure [20] showed that the OH radical intensity and burning velocity both increased with increasing H_2 content. Thus fuels with higher LCV and higher H_2 content will benefit combustion and burn out. Therefore, bituminous coal syngas with higher H_2 content and LCV has the strongest OH signal intensity compared with other syngases or even methane, creating better burn out.

For further direct comparison and quantitative analysis of the OH radical intensities between the different syngas types, more data were extracted and analyzed. The fluorescence intensity qualitatively reflects OH radical intensity because the $Q_1(8)$ line has been selected as the excited lower

energy level, for its insensitivity to temperature. Profiles of OH radical intensity along axial and radial directions (crossing lines in Figure 4(a)) were obtained from the averaged OH-PLIF images in Figure 4(a) and displayed in Figure 5. Figure 5(a) shows the OH radical intensity distribution along with the flow direction in the range 2*d*–16*d*. Bituminous coal syngas has clearly the strongest OH signal intensity while methane has the lowest. Figure 5(b) shows OH distributions along the radial direction between −3.5*d*–3.5*d*.

Figure 6 shows the widths of the central unburnt regions and the peak values of the OH signal intensities for the four typical syngases and methane. Methane had the widest central unburnt region and the weakest OH intensity compared to the four syngas types because of its more distinctive gas composition and combustion characteristics. The H_2/CO/CH_4 content affects the LCV of the fuel and N_2/CO_2 dilution reduces both the flame stability and OH relative intensity [21]. Among the four syngases, the width of the central unburnt region for the bituminous coal syngas is the narrowest, while the wood residue and corn core syngas show gradual increases, leaving wheat straw syngas with the largest value. It also can be observed that the peak OH radical intensity of the bituminous coal was 5080, which was much stronger than that for wheat straw at 4330. The H_2 content improves the diffusion property and narrows the central unburnt region. Bituminous coal syngas seems to be burning fastest with the strongest combustion intensity.

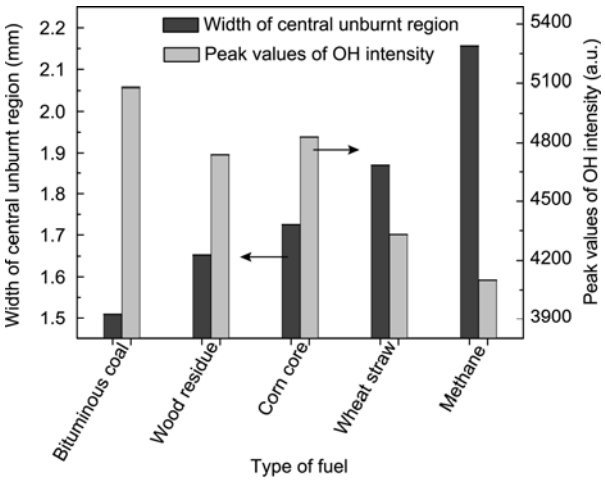

Figure 6 Width of the central unburnt region (left abscissa) and peak OH intensity (right abscissa) of the syngas flames.

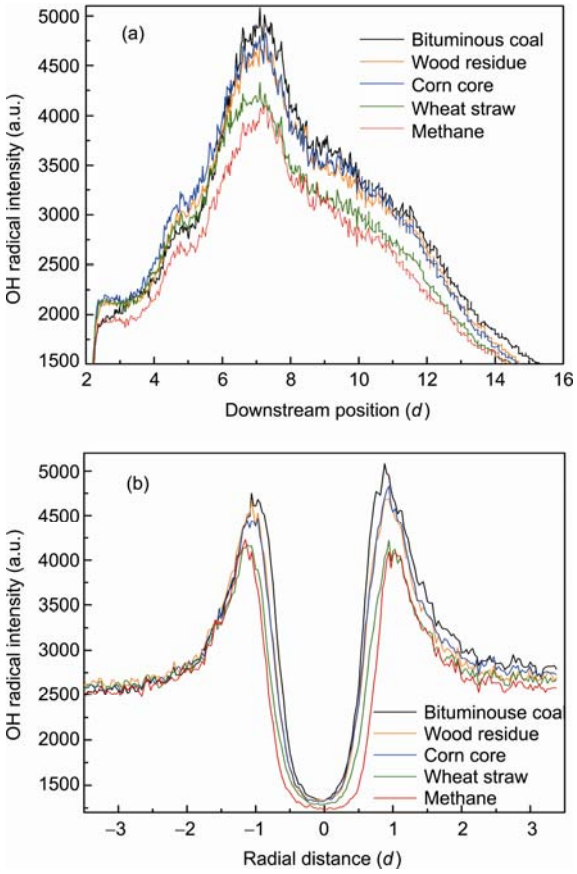

Figure 5 OH radical distributions of the syngas flames at Φ=0.8 and *Re* = 10000. (a) Axial distribution; (b) radial distribution.

2.3 Effect of turbulence intensity on OH radical distribution

Turbulence intensity is an important factor determining heat and mass transfer processes and subsequently the combustion characteristics. Figure 7 shows the instantaneous OH-

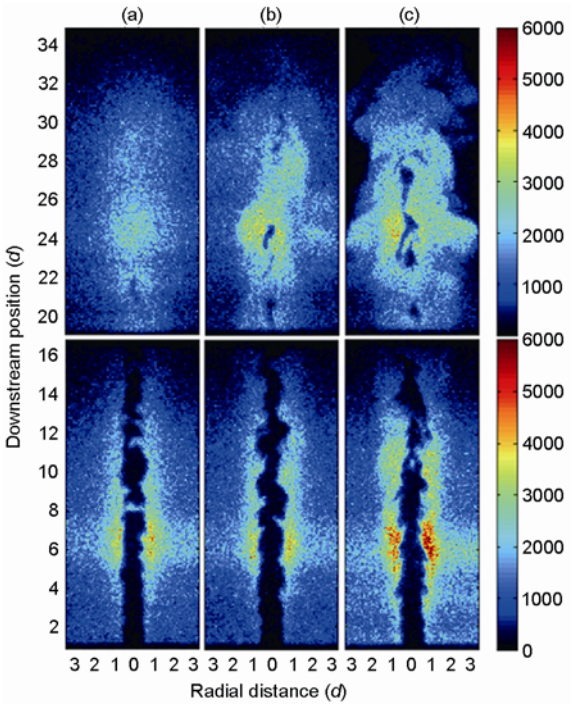

Figure 7 OH-PLIF images of bituminous coal syngas with different turbulent intensities.(a) *Re* = 5000; (b) *Re* = 10000; (c) *Re* = 15000.

PLIF images of the bituminous coal syngas flame at different Reynolds numbers ranging from $Re = 5000$ to $Re = 15000$. The combustion characteristics of syngas, such as flame location, flame structure, and the burnt and unburnt regions, were investigated. The equivalence ratio was maintained at 0.8.

At larger Reynolds numbers, the central flame front structures are observed in Figure 7 with more folded, larger curvatures and approximately larger brush thickness. Conventionally, the brush thickness is defined as twice the root-mean-squared value of the fluctuations of the radial position of the flame from its mean position [22]. In addition, more numerous foldings on a finer scale are seen between downstream positions 6*d*–14*d* than at smaller Reynolds numbers. Because of entrainment by the stronger turbulence intensity, mixing between the burnt and unburnt gas was enhanced through the small-scale vortex structures in turbulence. Therefore, the effect of turbulence on the flame propagation can be clearly seen from OH-PLIF images.

Some small holes in the central jet that are related to local extinctions can also be observed in Figure 7(c). Instantaneous local extinctions can be observed in the highly-turbulent (large Reynolds number) flames. The local flame structures will be of great interest in the further development of combustion models [17]. Some sharp cusps were also observed in the flame front, especially between downstream positions 4*d*–12*d*. In Figure 7(a), the central unburnt jet is seen to separate into two discontinuous parts at 8*d*. This occurrence is probably due to entrainment of the burnt hot flue gas by buoyancy causing the flame front to occasionally penetrate across the central jet fuel. Mungal et al. [23] have reviewed the observed appearance and characterized momentum-driven and buoyancy-driven flames.

Figure 8 shows the statistically-evaluated OH-PLIF images of bituminous coal gasification syngas flame with different turbulent intensities according to those conditions in Figure 7. The OH radical intensities all reached maximal values at downstream positions of about 6.6*d* because of the highly-folded flame structure and also uneven energy distribution of the laser beam. The OH radical reaction layer with the largest Reynolds number (right column in Figure 8(a)) was more convergent and narrower in the radial direction between downstream positions 6*d*–7*d* than at lower Reynolds numbers (left column). The increased turbulence intensity has enhanced the entrainment of ambient air and burnt flue gas in the flame front, thus "compressing" the flame and intensifying mixing and reactions [17]. Observed also in Figure 8(b) is the appearance of a stronger OH radical intensity in the flame for larger Reynolds numbers. The higher turbulence intensity intensifies heat and mass transfer processes, accelerating combustion.

The OH radical intensity and thickness of the OH reaction layer are important pieces information in describing combustion characteristics particularly when validating result from numerical simulations. Donbar et al. [22] have reported that flame surface density and the reaction layer

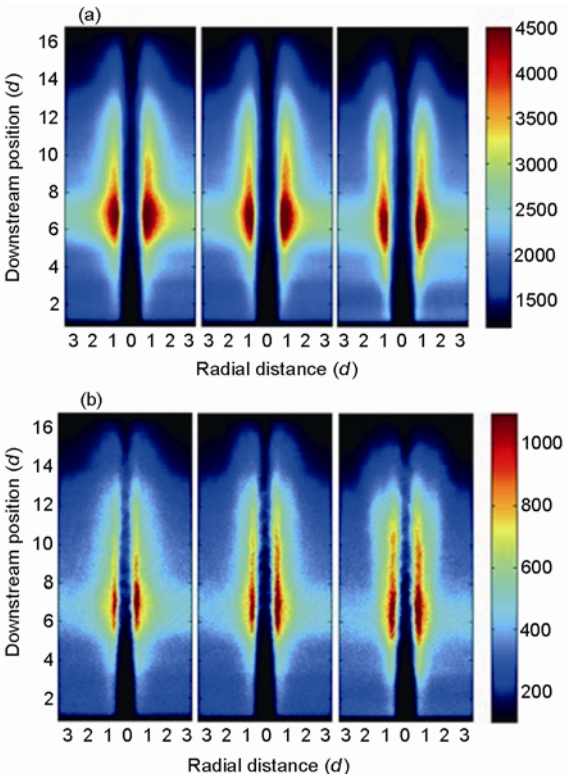

Figure 8 Reynolds number dependence in statistically-evaluated OH-PLIF images of bituminous coal syngas flame. (a) Ensemble average; (b) standard deviation. From left to right: $Re = 5000$, 10000, 15000.

thickness can be used to assess large eddy simulations (LES). Figure 9 shows the thickness of the OH radical reaction layers and peak values of OH signal intensity; with the Reynolds number increasing from 5000 to 15000, the thickness of OH layers decreases from 7.4 mm to 4.7 mm, in contrast, the peak value of the OH intensity increases from 5000 to 5040, although this increase is not very obvious compared with the thickness variety. The higher turbulence intensities compress the reaction layers and accelerate the chemical reactions, and hence intensify combustion.

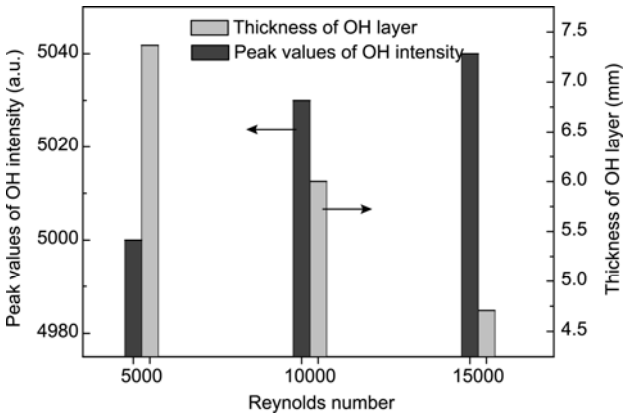

Figure 9 Thickness of OH layer and peak OH intensity of bituminous coal gasification syngas with different Reynolds number.

3 Conclusions

Lean premixed flame characteristics of several typical LCV syngases consisting of H_2, CO, CH_4, O_2, CO_2, and N_2 were investigated using advanced PLIF laser diagnostic technology. The methane/air flame provided a basis for comparison and validation. Results show that H_2 content, LCV, and turbulence intensity are the most effective factors influencing the OH radical intensity and the thickness of the OH radical layers. Bituminous coal gasification syngas with relatively higher LCV and H_2 content tended to burn out more easily. Through thickness variations in the OH radical layers and the signal intensities, turbulence intensities can compress reaction layers and intensify combustion processes in syngas. Furthermore, the structures of well-developed turbulence jet flames and turbulence-flame interactions were observed and characterized by OH imaging. The flame curvature (sharp cusp), local extinction (holes and penetration), OH layer thickness, and folding were analyzed with OH-PLIF instantaneous imaging and statistical results.

This work was supported by the National Natural Science Foundation of China (*50806066*)*, the National Basic Research Program of China* (*2009CB219802*) *and the Program of Introducing Talents of Discipline to University* (*B08026*).

1 Wang F R. The engineering analysis method of IGCC energy balance (in Chinese). Gas Turb Technol, 2001, 14: 43–45
2 Jiang J C. Prospect on research and development of biomass energy utilization (in Chinese). Chem Ind Forest Prod, 2002, 22: 75–80
3 Ma L Z, He P, Wang H, et al. Co-pyrolysis of coal/biomass (in Chinese). J Guizhou Chem Ind, 2004, 29: 20–23
4 Sun H Y, Yang S I, Jomaas G, et al. High-pressure laminar flame speeds and kinetic modeling of carbon monoxide/hydrogen combustion. Proc Combust Inst, 2007, 31: 439–446
5 Som S, Ramírez A I, Hagerdorn J, et al. A numerical and experimental study of counter-flow syngas flames at different pressures. Fuel, 2008, 87: 319–334
6 Prathap C, Ray A, Ravi M R. Investigation of nitrogen dilution effects on the laminar burning velocity and flame stability of syngas fuel at atmospheric condition. Combust Flame, 2008, 155: 145–160
7 Mclean I C, Smith D B, Taylor S C. The use of carbon monoxide/hydrogen burning velocities to examine the rate of the CO+OH reaction. Proc Combust Inst, 1994, 25: 749–757
8 Choudhuri A R, Subramanya M, Gollahalli S R. Flame extinction limits of H_2-CO fuel blends. J Eng Gas Turb Power, 2008, 130: 1–8
9 Charlston-Goch D, Chadwick B L, Morrison R J S, et al. Laser-induced fluorescence measurements and modeling of nitric oxide in premixed flames of CO-H_2-CH_4 and air at high pressures. Combust Flame, 2001, 125: 729–743
10 Dobbeling K, Eroglu A, Winkler D, et al. Low NO_x premixed combustion of MBtu fuels in a research burner. J Eng Gas Turb Power, 1997, 119: 553–558
11 Ouimette P, Seers P. Numerical comparison of premixed laminar flame velocity of methane and wood residue syngas. Fuel, 2009, 88: 528–533
12 Natarajan J, Lieuwen T, Seitzman J. Laminar flame speeds of H_2/CO mixtures: Effect of CO_2 dilution, preheat temperature, and pressure. Combust Flame, 2007, 151: 104–119
13 Natarajan J, Lieuwen T, Seitzman J, et al. Laminar flame speeds and strain sensitivities of mixtures of H_2 with CO, CO_2 and N_2 at elevated temperatures. In: Proceedings of ASME Turbo Expo, Montreal, Canada, 2007, GT-2007-27967
14 Ma L L, Wu C Z, Sun L, et al. Biomass Gasification Technology and Its Application (in Chinese). Beijing: Chemical Industry Press, 2003
15 Quang V N, Phillip H P. The time evolution of a vortex-flame interaction observed via planar imaging of CH and OH. Proc Combust Inst, Naples, Italy, 1996, 26: 357–364
16 Li G Q, Gutmark E J. Geometry effects on the flow field and the spectral characteristics of a triple annular swirler. In: Proceedings of ASME Turbo Expo, Atlanta, USA, 2003, GT2003–38799
17 Kiefer J, Li Z S, Zetterberg J, et al. Investigation of local flame structures and statistics in partially premixed turbulent jet flames using simultaneous single-shot CH and OH planar laser-induced fluorescence imaging. Combust flame, 2008, 154: 802–818
18 Kalmthout E V, Veynante D, Candel S M. Direct numerical simulation analysis of flame surface density equation in non-premixed turbulent combustion. Proc Combust Inst, 1996, 26: 35–42
19 Ding Y B, Sun J H, He X C, et al. Flame propagation characteristics and flame structures of zirconium particle cloud in a small-scale chamber. Chinese Sci Bull, 2010, 55: 3954–3959
20 He Y, Wang Z H, Yang L, et al. Study on Effects of H_2 Fraction and Turbulent Intensity on the Flame Structure of Typical Coal Gasification Syngas by OH-PLIF Measurements. In: Proceedings of the CSEE, Shanghai, China, 2010, 31: 28–33
21 Seo J I, Kim N I, Shin H D. An experimental study of the fuel dilution effect on the propagation of methane-air tribrachial flames. Combust flame, 2008, 153: 355–366
22 Donbar J M, Driscoll J F, Carter C D. Reaction zone structure in turbulent non-premixed jet flames-from CH-OH PLIF images. Combust Flame, 2000, 122: 1–19
23 Mungal M G, Karasso P S, Lozano A. The visible structure of turbulent jet diffusion flames-large-scale organization and flame tip oscillation. Combust Sci Technol, 1991, 76: 165–185